Editors' Suggestion

Spin-polarized quantized electronic structure of Fe(001) with symmetry breaking due to the magnetization direction

E. Młyńczak,[1,2,*] I. Aguilera,[1,†] P. Gospodarič,[1] T. Heider,[1] M. Jugovac,[1,‡] G. Zamborlini,[1,§] C. Tusche,[1,3] S. Suga,[1,4] V. Feyer,[1] S. Blügel,[1] L. Plucinski,[1] and C. M. Schneider[1,3]

[1]*Peter Grünberg Institut PGI, Forschungszentrum Jülich and JARA- Fundamentals of Future Information Technologies, 52425 Jülich, Germany*

[2]*Jerzy Haber Institute of Catalysis and Surface Chemistry, Polish Academy of Sciences, Niezapominajek 8, 30-239 Krakow, Poland*

[3]*Fakultät für Physik, Universität Duisburg-Essen, 47057 Duisburg, Germany*

[4]*Institute of Scientific and Industrial Research, Osaka University, Ibaraki, Osaka 567-0047, Japan*

(Received 10 November 2020; revised 22 December 2020; accepted 4 January 2021; published 20 January 2021)

Quantum well states formed by *d* electrons in metallic thin films are responsible for many fundamental phenomena that oscillate with layer thickness, such as magnetic anisotropy or magnetoresistance. Using momentum microscopy and angle-resolved photoemission, we mapped in unprecedented detail the quantized electronic states of Fe(001) in a broad photon energy range starting from soft x-ray (160 eV) down to vacuum ultraviolet (8.4 eV). We show that it is possible to simulate the experimentally observed photoemission spectra with high accuracy by using the *ab initio* electronic bulk band structure as the initial state, taking into account that free electron final electronic states are intrinsically broadened along the wave vector direction perpendicular to the sample surface. To simulate the thin-film case, we take into account a subset of the initial electronic states, which results in the reproduction of the quantized electronic structure observed in the experiment. In addition, we present results of the spin-sensitive measurements, which are confronted with the photoemission simulation that takes into account the spin degree of freedom. We demonstrate electronic states that can be responsible for the oscillations of the magnetic anisotropy in Fe(001) thin films with periods of about 5 and 9 monolayers. We show that these quantum well states change position in reciprocal space depending on the magnetization direction. Our photoemission simulation reproduces this effect, which highlights its origin in the relativistic bulk electronic band structure of bcc Fe. We also observed magnetization-dependent spin-orbit gaps with the symmetry lower than the bulk symmetry. We believe that the same method of simulating photoemission spectra might facilitate interpretation of the photoemission intensities measured for other three-dimensional materials, especially when the spin-polarized quantized electronic states are considered.

DOI: 10.1103/PhysRevB.103.035134

I. INTRODUCTION

Thin films can host quantum well states (QWS) as a result of the electron confinement in the direction perpendicular to the surface [1,2]. The confinement of the electronic states within the layer is ascertained when the respective states cannot couple to the electronic states outside. This is achieved naturally at surfaces (no states available at the vacuum side) and at interfaces with insulators and semiconductors. When metal-metal interface comes into play, the confinement near the Fermi level is possible when there are no states in the interfaced metal for certain values of the in-plane wave vector [3] or the available states differ in the symmetry of the wave function so that coupling with them is hindered.

Many collective properties of the thin-film layered systems are observed to oscillate with thickness of the constituents. This can be explained as a result of the QWS that cross the Fermi level periodically when the film thickness increases. The well-known examples include interlayer exchange coupling [4], giant magnetoresistance [5], tunneling magnetoresistance [6–8], and magnetic anisotropy [9–11].

QWS formed by Fe *d* states in Fe(001)/Ag(001) were shown to be responsible for magnetic anisotropy energy and orbital moment anisotropy oscillating with Fe thickness with a period of $\sim$ 5–6 monolayers (ML) [9–12]. In the experimental works, different quantized bulk electronic states were suggested to contribute to these oscillations [9–11]. However, in the theoretical work of Sandratskii [12] it was claimed that the oscillations cannot be explained based on the bulk band structure as it does not adequately reflect the properties of the 3*d* QWS in Fe. Instead, it was shown that the broad *k*-space region away from the $\overline{\Gamma}$ point of the surface Brillouin zone contributes the most to the anisotropy oscillations [12]. In the Fe/Au(001) multilayers, oscillations of the magnetic anisotropy energy both in sign and in magnitude with a period of about 8–10 ML were predicted by first-principles

*e.mlynczak@fz-juelich.de

†Current affiliation: IEK5-Photovoltaik

‡Current affiliation: Istituto di Struttura della Materia-CNR (ISM-CNR)

§Current affiliation: Technische Universität Dortmund

calculation [13]. It was speculated that such a substantial change in the anisotropy is related with the quantized electronic states that split in the magnetization-dependent manner [13].

Surprisingly, the experimental reports on the observations of QWS in the occupied part of the band structure of Fe are rather scarce. As notable examples we should mention a report on the development of QWS of a single spin (majority) character in Fe(110)/W(110) system [14] and demonstration that the density of states near the Fermi level oscillates with Fe thickness in Fe(001)/Ag(001) [10,11].

The Fe(001)/Au(001) system is a very good candidate to host QWS, thanks to the very small lattice mismatch between the two lattices as well as high flatness of Fe(001) films. What is more, the band structures of Fe and Au differ substantially, which allows the confinement of electronic states. The Fermi surface of Au is a single sheet, in a first approximation shaped as a sphere, made out of electronic states of *sp* character with necks around the [111] direction. This allows development of QWS of *d* character near the Fermi level within Fe films interfaced with Au. In Ref. [15] it was shown by inverse photoemission spectroscopy that unoccupied electronic states of Fe(001)/Au(001) develop QWS.

The dependence of the electronic structure of a ferromagnet on the magnetization direction is a fundamentally interesting issue, lying at the heart of many basic effects in magnetism, such as the existence of magnetocrystalline anisotropy [16]. First-principles electronic structure calculations show that a change of the magnetization direction can trigger a topological phase transition in mixed Weyl semimetals [17] or even a direct-to-indirect band-gap transition in a two-dimensional (2D) ferromagnet, CrI_3 [18]. In thick Fe films (100 ML) grown on Au(001), magnetization-dependent opening/closing of the spin-orbit gaps observed using angle-resolved photoemission spectroscopy was reported by some of us [19]. Such modifications of the electronic structure of Fe has been recently also recognized as a topological phase transition [20,21]. Moreover, since Fe/Au(001) is an example of a ferromagnet/heavy-metal system potentially interesting for spin orbitronics [22], it is worth asking a question whether the QWS formed within a thin Fe layer show asymmetric and magnetization-dependent band dispersions brought by the combined effect of the time-reversal and inversion symmetry breaking, similar to the ones found for Co/W(110) [23].

To draw a complete picture of the electronic band structure related effects, next to the high-resolution experiment, a suitable theoretical approach is needed. In the case of *k*-resolved photoemission spectroscopy from materials that exhibit a three-dimensional band structure, the most intriguing is the problem of the correct treatment of the wave vector perpendicular to the sample surface ($k_\perp$), which is not strictly conserved in the photoemission process. In case of the thin films which host QWS, $k_\perp$ is also quantized [1,24]. On top of that, the photoemission spectra are intrinsically broadened along $k_\perp$ direction [25,26].

The most accurate way to deal with the $k_\perp$ issue is to perform the one-step model of photoemission calculations, in which it is possible to model the surface barrier and consider the matrix elements of the possible electronic transitions [27]. A significant drawback of this method is, however, its complexity and the computational time demand. Therefore simplified approaches are often used. One of them would be to compare the measured spectra to a single cut in *k* space, at the well-defined $k_\perp$ value, which can be found following the approximation of a free-electron final-state model (FEFSM) [19,28–33]. Another approach, used especially for the thin films in which quantized states are present, would be to compare the measured spectra to the result of the *ab initio* band structure calculations in the slab geometry, which essentially contains all of the possible $k_\perp$ values [34–36].

In this article we demonstrate photoemission data which reveal in unprecedented detail the spin-polarized quantized occupied electronic band structure of Fe(001) with some of the QWS that visibly shift when the magnetization direction is switched. We demonstrate that these states could be responsible for the oscillations of the magnetic anisotropy with periods of ~ 5 and ~ 9 ML of Fe(001). We prepared Fe(001) thin films of nearly perfect quality by cold deposition on a Au(001) single crystal. The experiments were performed using a momentum microscope together with a synchrotron light source as well as in a laboratory-based angle-resolved photoelectron spectroscopy setup using a low-energy Xe excitation source. We compare the experimentally measured spin- and *k*-resolved photoemission intensities from Fe(001) with the simulations of the photoemission spectra that take into account intrinsic broadening along the $k_\perp$ direction as well as quantization of the bulk electronic states within the thin-film geometry. Thanks to that approach we are able to identify nearly all of the experimentally observed spectral intensities. We show that the magnetization-dependent shifts of the QWS are fully reproduced by our simulations, which highlights their origin in the relativistic bulk electronic structure of Fe. We also present the magnetization-dependent openings of the spin-orbit gaps which reveal the symmetry breaking due to the presence of the sample surface.

II. EXPERIMENTAL DETAILS AND PHOTOEMISSION SIMULATIONS

The 40- and 20-ML Fe films (1 ML = 1.43 Å) were grown *in situ* on Au(001) single crystal at low temperature ($T = 100$ K) using molecular beam epitaxy and gently annealed up to 570 K. This preparation procedure was found previously to result in high-quality Fe(001) films with no Au present on the Fe surface [19], in contrast to room-temperature deposition [37]. This was also confirmed by x-ray photoelectron spectroscopy measurements. Mapping of the electronic dispersions within the full Brillouin zone with photon energies of VUV up to the soft x-ray region (70–160 eV) was performed using the momentum microscope at the NanoESCA beamline in the Elettra synchrotron in Trieste (Italy) [38]. These measurements were performed using both *s*- and *p*-polarized light. The momentum microscope is equipped with a W(001)-based spin detector [39], which enables collecting constant energy spin-resolved maps within the entire Brillouin zone of Fe(001). The analysis of the spin-resolved data was performed following the procedure described in Ref. [40]. In addition, high-resolution spectra were taken using a laboratory-based unpolarized light source of low photon energy (8.4 eV). Before each measurement, the samples were

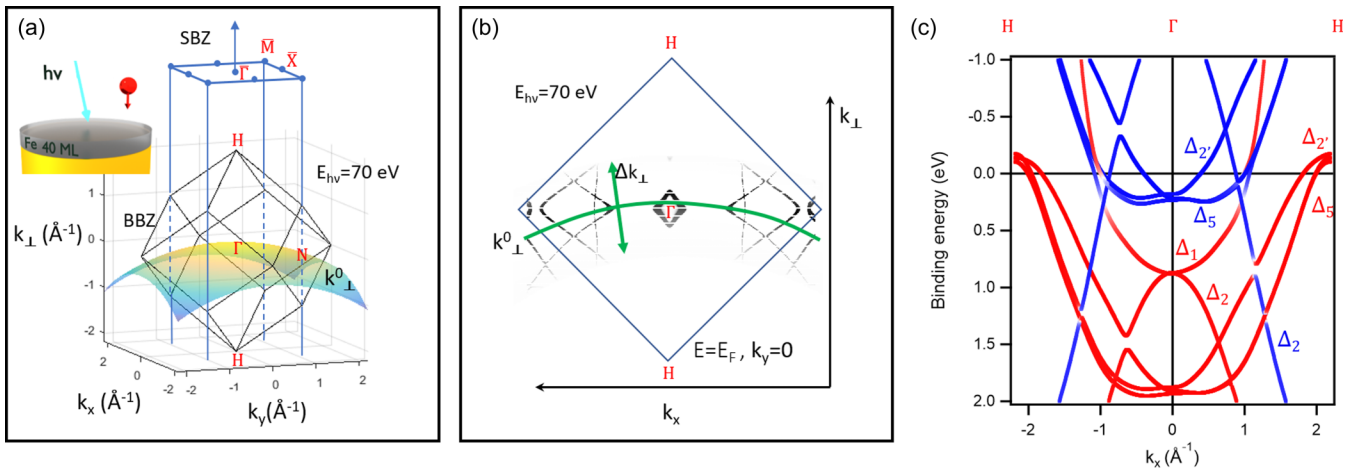

FIG. 1. (a) Bulk Brillouin zone (BBZ) of bcc Fe and surface Brillouin zone (SBZ) of Fe(001) with superimposed $k^0_\perp(k_x, k_y)$ surface which defines location of the initial electronic states that contribute to photoemission intensity according to free electron final-state model for photon energy of 70 eV. The inset shows a sketch of the photoemission experiment as seen in real space. (b) Illustration that schematically shows a range of the initial states involved in the photoemission simulation with respect to the size of the BBZ. (c) Relativistic GW bulk electronic structure of bcc Fe along Δ line of BBZ. Blue (red) color indicates predominantly minority (majority) states. Labels identify orbital symmetry. Negative (positive) k_x values correspond to direction along (perpendicular) to magnetization.

remanently magnetized using an oriented permanent magnet which was brought close to the sample surface.

Within an intuitive three-step model of photoemission [28], an electron is photoexcited from a certain initial Bloch state to a final state within the solid (step I). This transition is governed by the matrix element between the two states (M_{fi}). In the next step (step II) the excited electron travels a certain distance [on average, inelastic mean free path (IMFP)] before being emitted from a solid (step III).

In a photoemission experiment, schematically shown in Fig. 1(a), the electrons emitted at a certain emission angle (θ) can be identified as originating from the Bloch state of a strictly defined value of the in-plane wave vectors (k_x and k_y), depending on the photoemitted electrons' kinetic energy (E_{kin}): $k_{x(y)} = \sqrt{(2m/\hbar^2)E_{kin}}\sin\theta$. The out-of-plane momentum of the Bloch state $k_\perp$ is not directly measurable in the photoemission experiment. The actual initial-state perpendicular momentum $k^0_\perp$ can, however, be approximated, e.g., assuming that the final electron state is a free electron as in FEFSM. Then $k^0_\perp$ can be found as (V_0 stands for the value of the inner potential)

$$k^0_\perp = \sqrt{(2m/\hbar^2)(E_{kin}\cos^2\theta + V_0)}. \quad (1)$$

An exemplary $k^0_\perp(k_x, k_y)$ cut superimposed on the sketch of the Brillouin zone of bcc Fe that corresponds to the photoemission induced by light of an energy $h\nu = 70$ eV is shown in Fig. 1(a). The $k_\perp$ problem in photoemission is not limited to finding $k^0_\perp$. Another fundamental issue is the intrinsic broadening of the photoemission spectra along the $k_\perp$ direction [25,26]. This intrinsic broadening is a final-state effect which, within the three-step model of photoemission, can be related to the escape depth of the photoexcited electron. When taken more rigorously, as in the one-step formalism, the final state should be treated as a so-called inverse-LEED state, corresponding to the plane wave damped exponentially as a result of the limited lifetime and multiscattering processes [28]. In each case the final state should be imagined as being spatially extended in the subsurface region. This spatial extension defines the uncertainty of an electron's location in the direction perpendicular to the sample surface which, in turn, can be translated to the uncertainty of the $k_\perp$ vector ($\Delta k_\perp$) via the Heisenberg uncertainty principle.

The distribution of the $k_\perp$ vector is a Lorentzian centered at $k^0_\perp$ [25]:

$$L = \frac{\Delta k_\perp}{2\pi}\frac{1}{(k_\perp - k^0_\perp)^2 + (\Delta k_\perp/2)^2}. \quad (2)$$

The *initial* − *state* spectral function is characterized by the Lorentzian distribution in energy centered at the band energy $[E^i(k^0_\perp)]$ due to the finite hole lifetime (τ_h), where $\Delta E = \hbar/\tau_h$ [25,26]:

$$A^i(E) \propto \frac{\Delta E}{[E^i - E^i(k^0_\perp)]^2 + (\Delta E/2)^2}. \quad (3)$$

To obtain the photoemission intensity, the initial-state spectral function must be integrated in $k_\perp$ [25,26]:

$$I(E^f, E^i) \propto \int_{-\infty}^{\infty} dk_\perp \mid T^f \mid^2 \mid M_{fi}(k_\perp) \mid^2 \times \frac{\Delta k_\perp}{(k_\perp - k^0_\perp)^2 + (\Delta k_\perp/2)^2} \times \frac{\Delta E}{[E^i - E^i(k^0_\perp)]^2 + (\Delta E/2)^2}. \quad (4)$$

In our simulations, we assume the final-state surface transmission (T^f) and photoexcitation matrix elements (M_{fi}) to be equal to unity. We will comment on the role of the matrix elements when discussing comparison of the simulations to the experimental results obtained using *p*- and *s*-polarized light. Since we are dealing here with the relative thick films, we do not take into account the $k_\perp$ broadening of the initial state related to the total film thickness [42], which equals

$\sim$0.05 Å^{-1} for a 40-ML-thick film. This is much smaller than the final-state $k_\perp$ broadening and therefore does not significantly influence the simulation result. $E^i(k_\perp^0)$ is an input to the simulation given by the result of the *ab initio* calculation of bulk electronic structure. Here we use the *GW* approximation of many-body perturbation theory that corrects the results from the generalized gradient approximation (GGA) functional of density functional theory.

To reconstruct the experimentally observed QWS, the photoemission simulations must include quantization of $k_\perp$. In general, comparison of the theoretical calculations of the bulk electronic band structures with the results of the slab calculations gives a picture of the direct correspondence of the discrete electronic states of the slab to the points on the bulk electronic dispersions [24]. Also, analysis of the photoemission from the QWS of thin films is a well-known method of recovering the bulk dispersions [1,24,43]. Therefore, in our photoemission simulation we quantized the electronic states of the bulk crystal along the Fe[100] direction. For such a quantization, one requires that a de Broglie wave associated with the electron forms a standing wave within the potential well of the width equal to the film thickness. We assume that the phase shifts at substrate-film and film-vacuum interfaces are equal to zero (or 2π) [1]. Therefore we use discrete values of $k_\perp$, the number of which equals the number of layers in the thin film.

In addition, to address the spin-resolved experimental result, we also included the spin degree of freedom in our photoemission simulations. To achieve that we first considered separately all the initial electronic states of predominantly minority (majority) character which contribute to the calculated photoemission intensity at each value of the parallel wave vector (k_x, k_y) [$I_{\min}(I_{\mathrm{maj}})$, respectively]. Then we simply calculated the spin polarization as

$$P = \frac{(I_{\min} - I_{\mathrm{maj}})}{(I_{\min} + I_{\mathrm{maj}})}. \tag{5}$$

A simplified sketch of the photoemission simulation that we perform here is presented in Fig. 1(b), where $k_\perp^0$ is indicated by a green solid line, while a double arrow spans $\Delta k_\perp$. In the following we will analyze the photoemission spectra from the direct vicinity of the Fermi level, where the photohole lifetimes are very long, with the resulting negligible initial-state energy broadenings. Therefore we assume that all the electronic states have the same energy broadening dominated by the experimental energy resolution. Lifetime broadening of the electronic band structure and correlation effects, significant below the Fermi level, have been described before for the same sample system [32].

The *GW* calculation was performed within the all-electron full-potential linearized augmented-plane-wave (FLAPW) formalism as implemented in the FLEUR [44] and SPEX [45] codes. The calculation was performed on a $10 \times 10 \times 10$ k-point mesh, which was enough to converge both eigenvalues and theoretical Fermi energy. However, for the photoemission simulation, a much denser mesh of $200 \times 200 \times 200$ k points was essential for reproducing the experimental results. Therefore we made use of the Wannier interpolation technique [46] to generate the data on the required k-point mesh. The Wannier functions were obtained with the WANNIER90 library [47]. The GGA calculation providing the input wave function and electronic quantities to the *GW* calculations was performed with an angular momentum cutoff of $l_{\max} = 8$ in the muffin-tin spheres and a plane-wave cutoff of 5.0 bohr^{-1} in the interstitial region. The $3s$ and $3p$ orbitals were treated as *semicore* by the use of local orbitals. The mixed product basis [45] used in the *GW* calculation was constructed with an angular momentum cutoff of 4 and a plane-wave cutoff of 3.0 bohr^{-1}. We used 170 unoccupied bands and two local orbitals per angular momentum up to $l = 3$ to describe high-lying states accurately and to avoid linearization errors [48]. The *GW* bulk bcc Fe electronic band structure along the Δ line is shown in Fig. 1(c).

All the photoemission simulations shown in this work were generated using a consistent set of parameters: the inner potential $V_0 = 11$ eV and the work function $W_f = 4.5$ eV. The broadening along $k_\perp$ direction ($\Delta k_\perp$) was used as a free parameter, adjusted until the best agreement with the experimental result was achieved. The values of $\Delta k_\perp = 0.33$ Å^{-1}, $\Delta k_\perp = 0.25$ Å^{-1}, and $\Delta k_\perp = 0.1$ Å^{-1} were found for $E_{h\nu} =$ 70, 160, and 8.4 eV, respectively. Such $k_\perp$ broadening constitutes from 4% ($E_{h\nu} = 8.4$ eV) up to 15% ($E_{h\nu} = 160$ eV) of the bulk Brillouin zone size. Such values of $\Delta k_\perp$ are in a very good agreement with those reported earlier for Fe(110) [49]. The values of $\Delta k_\perp$ can be translated to the corresponding IMFP values via the Heisenberg uncertainty principle. We find IMFP equal to 3, 4, and 10 Å for $E_{h\nu} = 70$, 160, and 8.4 eV, respectively. These values follow the universal curve reasonably well [50]. The energy broadenings of 50 and 10 meV were used to reconstruct the spectra measured using the momentum microscope [$E_{h\nu} = 70$ eV and $E_{h\nu} = 160$ eV presented in Figs. 4, 5, and 6] and laboratory-based Xe lamp [$E_{h\nu} = 8.4$ eV, Figs. 7 and 8], respectively.

III. RESULTS AND DISCUSSION

We start from presenting the three-dimensional representation of the electronic states of bcc Fe as given by the result of the *GW* calculation. The electronic states at binding energy of $E_b(\mathrm{GW}) = 0.095$ eV (with respect to the theoretical Fermi level) within the bulk Brillouin zone are presented in Fig. 2. This binding energy corresponds to the binding energy of $E_b = 0.05$ eV in the experimental result, which will be presented and discussed below (Fig. 4). We use the notation H_n, where $n = 1$–5, to highlight the inequivalence of the bulk H points, which arises as a result of the spin-orbit interaction in the presence of the magnetization vector that breaks the symmetry due to a selection of a magnetization direction [19] [Fig. 2(a)]. The H_5 point is located behind the image plane and therefore not visible in Fig. 2(a). The magnetization points along $H_5 - \Gamma - H_3$, which is indicated in Fig. 2(a) by a blue arrow. The $E_b(\mathrm{GW}) = 0.095$ eV constant energy surface is composed of five bands (band 5 to band 9), each depicted in superposition in Fig. 2(a) and individually in Figs. 2(b)–2(f). Except for some details, the presented constant energy sheets correspond to the Fermi surface of bcc Fe. It is worth noting that the theoretical Fermi level is crossed by one more band (band 10) that forms a Fermi sheet surrounding the bulk Γ point (not shown). Except for that, the

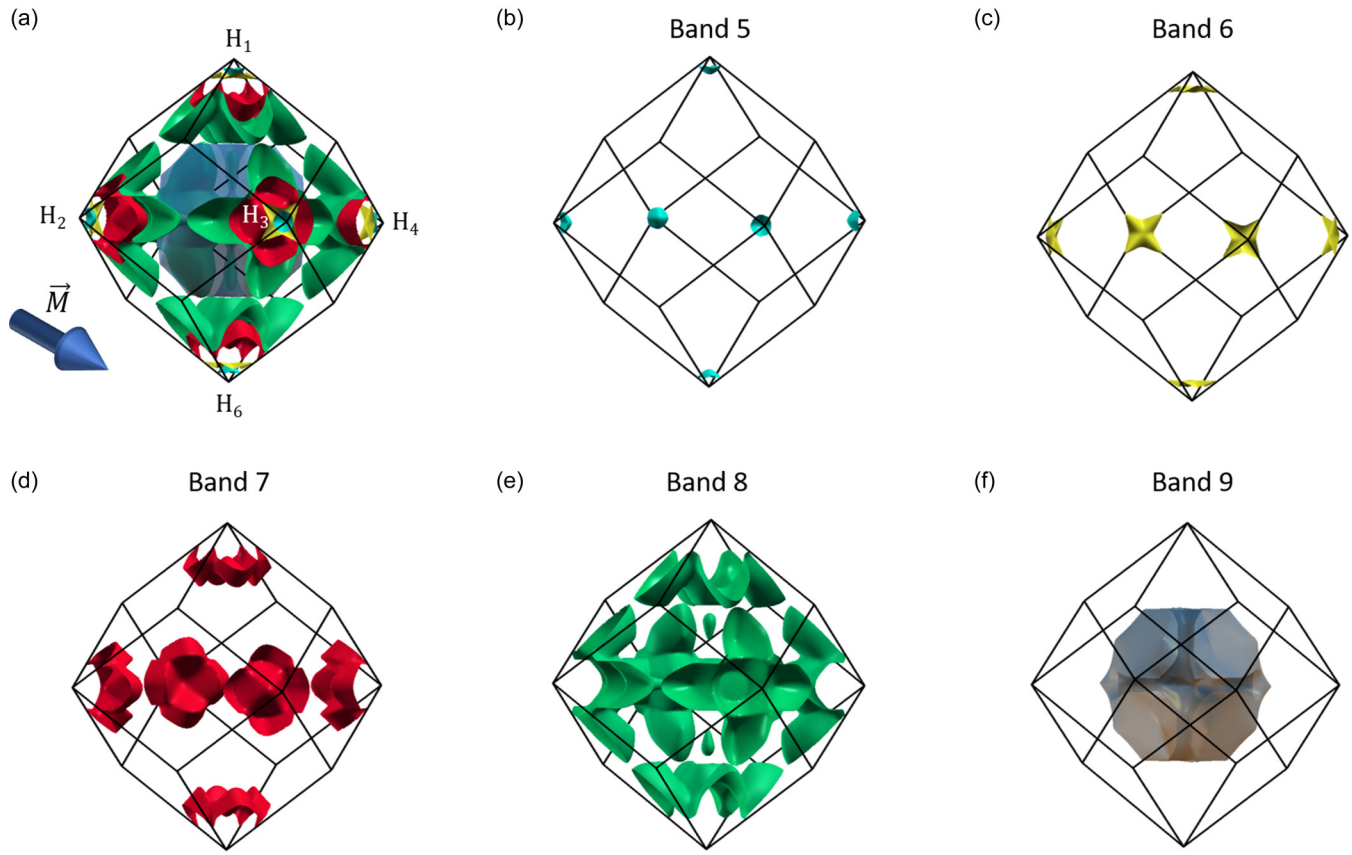

FIG. 2. Theoretical constant energy surfaces of bcc Fe at $E_b(\mathrm{GW}) = 0.095$ eV with respect to the theoretical Fermi level: (a) superposition of all the bands, (b–f) individual constant energy sheets of bands 5–9. Band 9 is depicted semitransparent. A blue arrow in (a) represents the magnetization direction. The figures were prepared using XCRYSDEN software [41]

most pronounced difference between the energy of $E_b(\mathrm{GW}) = 0.095$ eV and $E_b(\mathrm{GW}) = 0.0$ eV (theoretical Fermi level) as well as $E_b(\mathrm{GW}) = 0.045$ eV (experimental Fermi level) is the shape of the constant energy sheet of band 8. This is presented in Fig. 3, where we used a different view point than in Fig. 2 to clearly visualize the central part of the Brillouin zone. This sheet at $E_b(\mathrm{GW}) = 0.095$ eV develops a diamondlike shape that surrounds the bulk Γ point [Fig. 3(c)], which is not visible

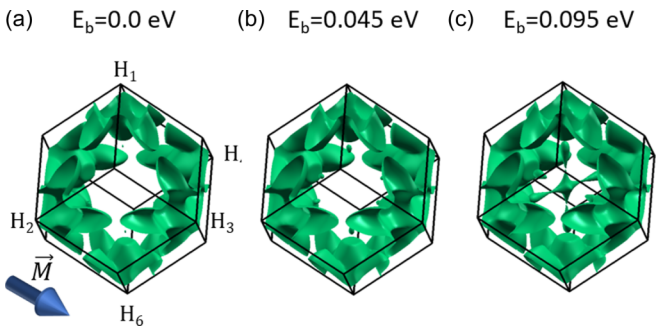

FIG. 3. Constant energy sheets formed by band 8 at different binding energies: (a) $E_b = 0.0$ eV (*GW* Fermi level), (b) $E_b = 0.045$ eV (experimental Fermi level), and (c) $E_b = 0.095$ eV (binding energy of experimental constant energy maps presented in Fig. 4). A blue arrow in (a) represents the magnetization direction. The figures were prepared using XCRYSDEN software [41].

at the theoretical Fermi level [Fig. 3(a)]. The constant energy sheet of band 8 is highly anisotropic at $E_b(\mathrm{GW}) = 0.095$ eV [Fig. 3(c)]. In the shape of the constant energy sheet formed by band 8, the $H_5 - \Gamma - H_3$ direction is distinguished—along that direction dropletlike shapes are visibly disconnected from the central diamondlike shape [Fig. 3(c)]. Interestingly, we performed measurements for different in-plane easy magnetization directions of the sample, but we did not experimentally observe this particular asymmetry. The experimental results obtained for a 40-ML-thick Fe(001) film using photon energies of $E_{h\nu} = 70$ and 160 eV of *p*- and *s*-linear polarizations are presented in Figs. 4(a), 4(b), 4(e), and 4(f). Judging the photoemission intensity, constant energy maps collected slightly below the Fermi level, i.e., at $E_b = 0.05$ eV, were chosen for the presentation. These constant energy maps qualitatively represent the Fermi surface of bcc Fe. Before each measurement the sample was magnetized; the magnetization direction is indicated in Fig. 4(a) by a blue arrow.

In order to identify the experimentally observed intensities, we start from comparing the experimental result to the *GW* bulk electronic band structure of bcc Fe near the Fermi level (Fig. 2), out of which we derive simple (k_x, k_y) cuts at well-defined $k_\perp$. According to the free-electron final-state model, photons of $E_{h\nu} = 70$ and 160 eV induce photoemission from the bcc Fe initial states located close to the Γ and *H* points within the bulk Brillouin zone, respectively. Corresponding cuts through the *GW* band structure are presented in Figs. 4(c)

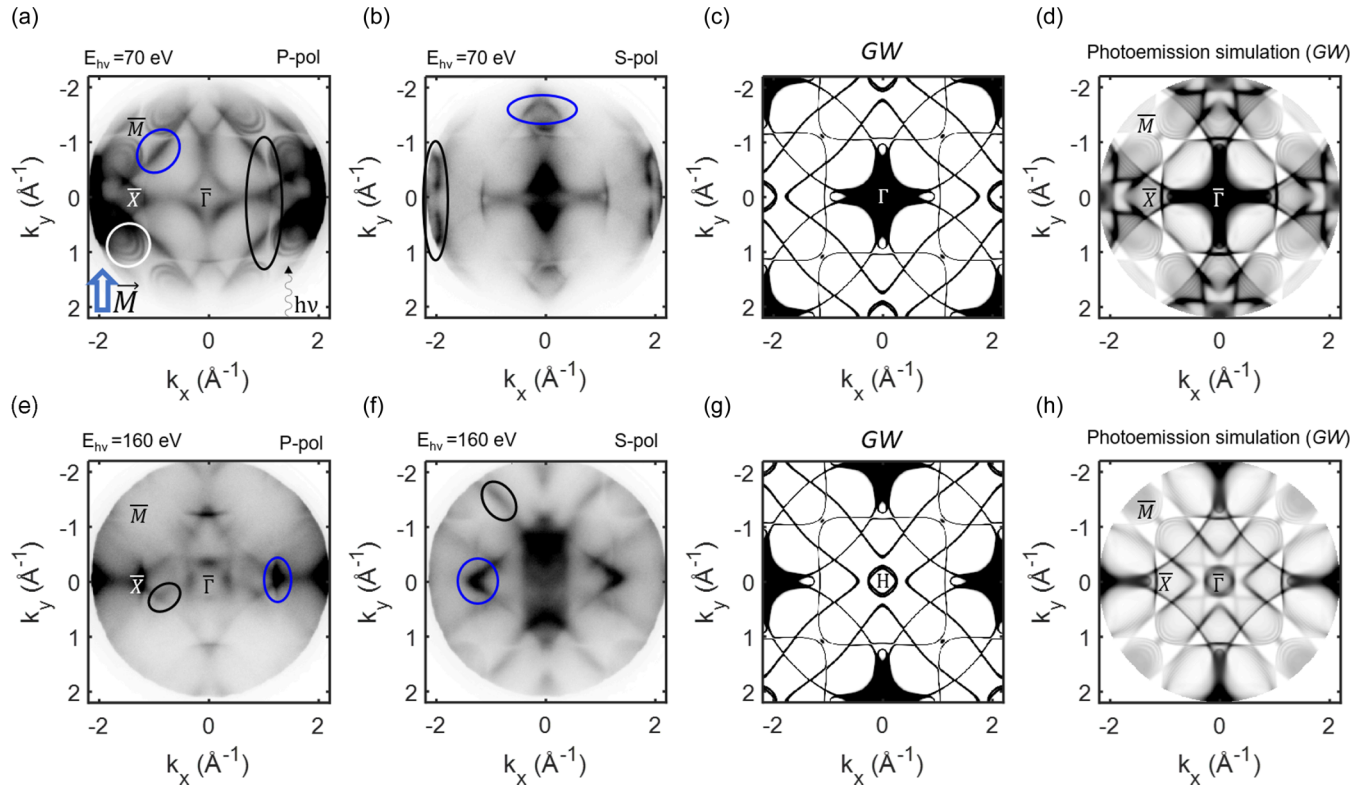

FIG. 4. Comparison of the photoemission intensities obtained using *p*- and *s*-polarized light of $E_{h\nu} = 70$ eV and $E_{h\nu} = 160$ eV for binding energy of $E_b = 0.05$ eV for the 40-ML-thick sample with electronic states within a single cut through the k space as defined by FEFSM as well as with the results of the photoemission simulations. (a, b) Experimental result for $E_{h\nu} = 70$ eV and *p*- and *s*-polarized light, respectively. A blue arrow represents the magnetization direction, a wiggly arrow shows the photon incidence direction. (c) Corresponding single cut through the k space, (d) corresponding result of the photoemission simulation. (e, f) Experimental result for $E_{h\nu} = 160$ eV and *p*- and *s*-polarized light, respectively, (g) corresponding single cut through the k space, and (h) corresponding result of the photoemission simulation. Colored ellipsoids mark the features of interest discussed in the text.

and 4(g). The width of the lines reflects the experimental energy broadening.

We can easily identify most of the experimental photoemission intensities for $E_{h\nu} = 70$ eV and *p*-polarized light [Fig. 4(a)] as originating from the constant energy sheet of band 8. We observe also high spectral intensity near the $\overline{M}$ point that can be identified as belonging to band 9 [marked by a blue ellipsoid in Fig. 4(a)]. The measurement performed using *s*-polarized light [Fig. 4(b)] reveals a substantially different picture, which highlights the role of the dipole transition matrix element. A characteristic diamondlike shape around $\overline{\Gamma}$ as well as thin lines near $\overline{X}$ that belong to band 8 are observed. The shapes characteristic for band 7 are marked by a blue ellipsoid. The intensities near the $\overline{M}$ points are fully suppressed. The experimental result for $E_{h\nu} = 160$ eV and *s*-polarized light [Fig. 4(f)] is dominated by the contribution of bands 8 and 9, which are marked by blue and black ellipsoids, respectively. High spectral intensity in the center of the image could be attributed to bands 5 and 6; however, here the agreement between the theoretical prediction and the result of the measurement is poorer. In the result for $E_{h\nu} = 160$ eV and *p*-polarized light [Fig. 4(e)], spectral intensity from band 8 is visible, but only near the $\overline{X}$ points (marked by a blue ellipsoid). A weak signal originating from band 7 is also observed (black ellipsoid), as well as features that can be identified as originating from bands 5 and 6 (around $\overline{\Gamma}$).

Clearly, there is a good correspondence between the theoretical cuts through the electronic band structure and the experimental result in terms of the general shape of the constant energy sheets. However, there are some interesting features in the experimental result which are not reproduced in the simple cuts through the bulk electronic band structure. Most importantly, the experimental result obtained for $E_{h\nu} = 70$ eV and *p*-polarized light [Fig. 4(a)] reveals concentric rings of the shape of band 8, which we identify as QWS [marked by a white circle in Fig. 4(a)]. To reproduce this experimental result, photoemission simulation must be invoked [Figs. 4(d) and 4(h)].

We see that most of the experimentally observed intensity variations at the Fermi surface directly correspond to the partial density of quantized initial states of the bulk crystal. Especially striking is that the regions of reduced intensity in the experimental map measured using *p*-polarized light and $E_{h\nu} = 70$ eV [Fig. 5(a)] and also *s*-polarized light and $E_{h\nu} = 160$ eV are fully explainable by the projected initial band structure [Figs. 4(d) and 4(h), respectively]. Also, e.g., features that resemble vertically oriented eyeglasses at the sides of the constant energy map in Fig. 4(b) (marked by a black ellipsoid) are perfectly reproduced by the photoemission simulation. The simulation is much better in this case than the single cut through k space [Fig. 4(c)] because the single cut is a simple flat cut (the same $k_\perp$ for each k_x, k_y), while

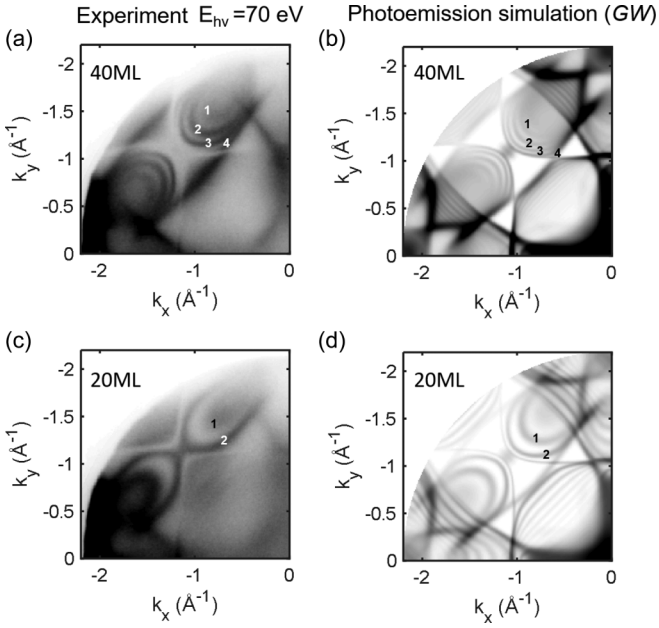

FIG. 5. Quantum well states near the Fermi level ($E_b = 0.05$ eV). Comparison of the photoemission intensities obtained using *p*-polarized light of $E_{h\nu} = 70$ eV for 40-ML-thick sample (a) and 20-ML-thick sample (c). The magnetization direction and the photon incidence direction are the same as in Fig. 4. (b, d) Corresponding photoemission simulations. The numerals mark corresponding quantum well states.

the photoemission simulation includes the actual curvature of $k_\perp^0$ as depicted in Fig. 1.

The biggest strength of our photoemission simulations is revealed in the very good reproduction of the quantized states of band 8, which are marked in Fig. 4(a) by a white circle. We take a closer look at the quantized states in Fig. 5, where we show the blowups of the *k*-space region where QWS are present. For the film thickness of 40 ML we observe four distinct QWS, which is depicted in Fig. 5(a). The number of QWS depends on the thickness of the film—the thicker the film, the more states fit into the potential well. ($k_\perp$ becomes continuous in the bulk limit; compare, e.g., Ref. [51] for an instructive demonstration of a band formation in a periodic system.) To demonstrate the thickness dependence of the QWS, we show the experimental result measured for a thinner sample, of half the thickness, i.e., 20 ML [Fig. 5(c)]. As expected, a thinner film shows a smaller number of QWS, in this case only two. We see that the number and separation of the QWS is well-reconstructed in the simulation [Figs. 5(b) and 5(d)]. In the experimental result of $E_{h\nu} = 70$ eV the only visible QWS are those formed within band 8; the other electronic states seem not to be quantized. Also, no QWS are visible in the measurement of $E_{h\nu} = 160$ eV. The reason for that might be the separation of the quantum wells, both in energy and in momentum, below the experimental resolution. It is interesting to note that even band 8 does not appear to be quantized when measured using $E_{h\nu} = 160$ eV [Fig. 4(f)]. The reason for this lies apparently in the quantities not captured by our photoemission simulation, such as the photon-energy-dependent cross section for photoemission [42].

In addition, we performed the magnetization-dependent and spin-resolved experiments. We define the magnetization direction UP, DOWN, RIGHT, and LEFT for the magnetization vector pointing along Fe[100], Fe[$\bar{1}$00], Fe[010], and Fe[0$\bar{1}$0], respectively. In Fig. 6 we present the results obtained for the sample magnetized DOWN [Fig. 6(a)] and UP [Figs. 6(b) and 6(c)]. To represent the spin-resolved data we use a two-dimensional color map, where the predominantly minority (majority) states are marked in blue (red) for the magnetization UP, while the color saturation represents the photoemission intensity. Note that the black color represents a fully spin-mixed state (spin polarization equal to zero). We see that the QWS of band 8 has the majority character while the central diamondlike shape has a minority character. The result of the spin-resolved photoemission simulation is presented in Fig. 6(d). It is encouraging to see a very good agreement between the experimental result and the theoretical simulation also in terms of the spin polarization of the respective sheets. Note that the approach that we use to calculate spin polarization reflects averaging of the spin information within the probed range of the perpendicular wave vector. This means that if accidentally the bands of the opposite spin happen to be present at the same binding energy for the same values of the parallel wave vector (k_x, k_y) within the $\Delta k_\perp$ range, the resulting measured spin polarization is reduced. This can be observed, e.g., within the region marked by a black circle in Fig. 6(d), where a grayish color represents substantially reduced spin polarization, which is in agreement with the experimental result [Fig. 6(b)].

In the same sample system for sample thickness of 40 ML we also observed QWS formed by bands 5 and 6 when we performed laboratory-based experiments using Xe excitation light source of $E_{h\nu} = 8.4$ eV. The result of this experiment is presented in Figs. 7(a) and 7(b), where reconstructed constant energy cuts (a) and electronic dispersions (b) close to the $\bar{\Gamma}$ point are presented. Small photon energy limits the accessible fraction of the *k* space and at the same time results in a high-wave-vector resolution. Here we also observe clear, well-separated QWS. These experimental results can be very well reconstructed by our photoemission simulation, the result of which is shown in Figs. 7(c) and 7(d). We use colored dots as a guide to the eye to help identify respective states. It is not straightforward to disentangle the visible states into QWS of bands 5 and 6, but we can achieve that thanks to the comparison with the photoemission simulation and single cuts through the *k* space (not shown). We mark the QWS of band 5 with a green dot, while a black dot marks the QWS of band 6. White and red dots mark the places where bands 5 and 6 meet. The observed states have prominent energy dispersion; note that the total energy range displayed in the image equals only 50 meV, the value of the energy resolution of the experiment performed using the momentum microscope [Figs. 4(a), 4(b) 4(e), 4(f)]. This experimental result allowed us to precisely determine the experimental Fermi-level position with respect to the result of the *GW* calculation $E_F(\text{exp}) = 0.045$ eV. We mark the experimental Fermi-level position by a horizontal red solid line in Fig. 7(d).

Importantly, bands 5 and 6 that are shown here to be quantized are present along the Δ line ($H - \Gamma - H$) of the bulk Brillouin zone, which corresponds to the [001] direction in

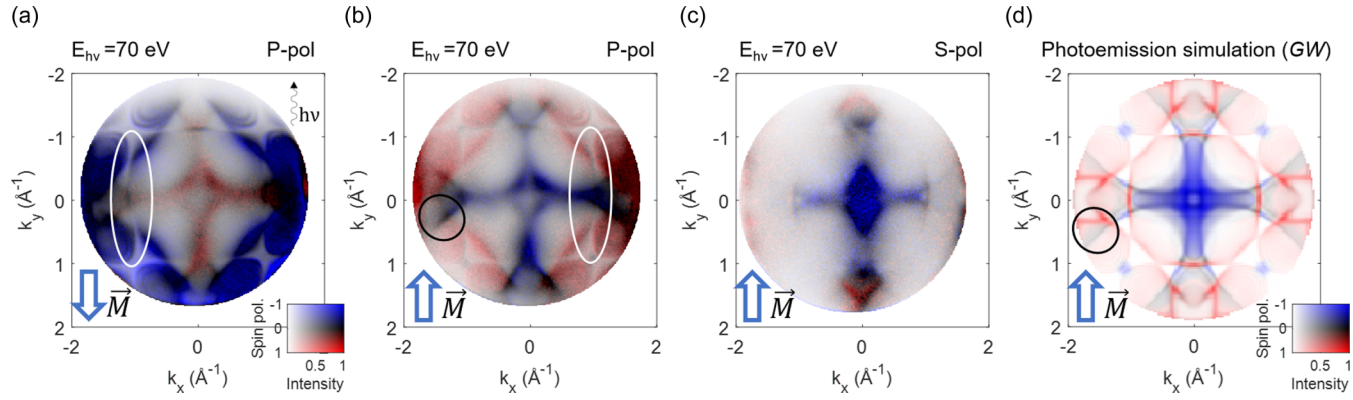

FIG. 6. Comparison of the spin-resolved photoemission intensities with the spin-resolved photoemission simulation. The experimental results are the constant energy cuts ($E_b = 0.1$ eV) measured using light of $E_{h\nu} = 70$ eV for a 40-ML-thick sample and (a) p polarization when the sample was magnetized DOWN, (b) p polarization when the sample was magnetized UP, and (c) s polarization when the sample was magnetized UP. A wiggly arrow in (a) indicates the photon incidence direction. (d) Result of the spin-polarized photoemission simulation. The two-dimensional color map shown in the insets is the same for all the figures. Blue and red color in (b–d) indicate predominantly minority and majority spin states, respectively. Black and white ellipses indicate features of interest discussed in the text.

the real space and can therefore contribute to the oscillations of the magnetic anisotropy energy in Fe(001) thin films. These states correspond to majority states Δ_5 and Δ_2', respectively, [compare Fig. 1(c)]. Out of *GW* calculation we find the Fermi wave vectors of these states along the quantization direction and at the experimental Fermi level equal to 1.76 and 1.95 Å^{-1}.

The wave function of a quantum well state consists of a fast oscillating Bloch function modulated by an envelope function which assures that boundary conditions are met at the interfaces [24]. The origin of the envelope function can be understood as a result of the superposition of two characteristic wavelengths: one related to the Fermi wavelength and the other to the lattice constant. The resulting beat frequency determines the frequency of the oscillations of physical properties of a quantum well system [52]. The wave vector of the envelope function can thus be found as $k_{env} = k_{ZB} - k_{Fermi}$, where k_{ZB} is the wave vector at the zone boundary and k_{Fermi} is the Fermi wave vector [24]. The envelope function defines the oscillation period: $p = \pi/k_{env}$. QWS formed by bands 5 and 6 would then be responsible for the oscillations of the macroscopic physical properties of the period equal to 5.1 and 9.1 ML, respectively. If we would assume the theoretical Fermi level, the corresponding result would read 6.8 and 10.9 ML, respectively. As pointed out in the Introduction, in the Fe(001)/Ag(001) system, magnetic anisotropy was found to oscillate with film thickness with the period of approximately 5–6 ML [9–11], which suggest that the QWS formed by band 5 of dominantly majority character and Δ_5 symmetry along the $H - \Gamma - H$ direction might be the origin of the oscillations, which is in accordance with the conclusion of Ref. [11]. Also, first-principles calculations of the magnetic anisotropy in Fe/Au(001) multilayers have shown oscillations with roughly 8–10-ML period [13]. Such oscillations might originate from the QWS of band 6, i.e., the majority Δ_2' electronic state.

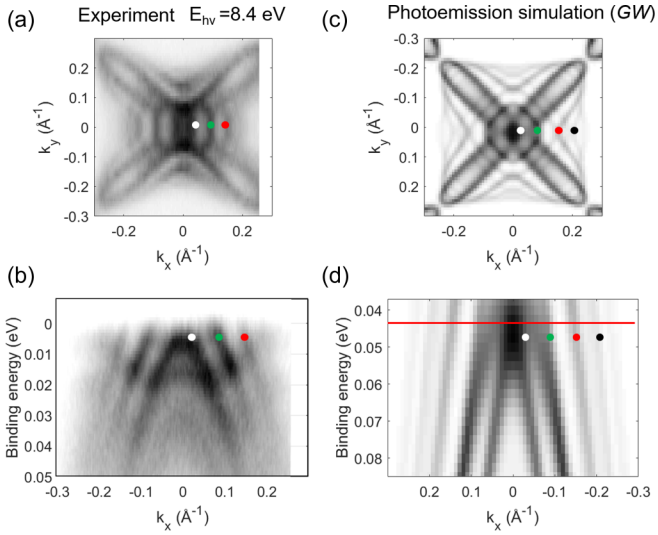

FIG. 7. Comparison of the photoemission intensities obtained using unpolarized light of $E_{h\nu} = 8.4$ eV for a 40-ML-thick sample with the photoemission simulation. (a) Experimental constant energy cut near the Fermi level ($E_b = 0.005$ eV). (b) Experimental dispersion. (c, d) Results of the photoemission simulation. Red horizontal line in (d) indicates position of the experimental Fermi level. Colored dots indicate corresponding quantum well states.

Note that both the experiment and the photoemission simulation revealed a substantial asymmetry within the constant energy cut—the shape around $\bar{\Gamma}$ is elongated along the k_y direction [Figs. 7(a) and 7(c)]. To investigate the origin of this asymmetry, we performed additional measurements, changing the magnetization direction of the sample. The obtained dispersions are presented in Fig. 8. Red dashed lines in the insets in Fig. 8 indicate k-space cuts with respect to the magnetization direction (shown by an arrow). We use colored dots as a guide to the eye to help identify the corresponding states. In the experimental result we can distinguish two types of spectra—results for magnetization UP and DOWN belong to the first type, while RIGHT and LEFT to the second one. We observe that in the second case, the QWS change position with respect to the magnetization; the distance in the k-space

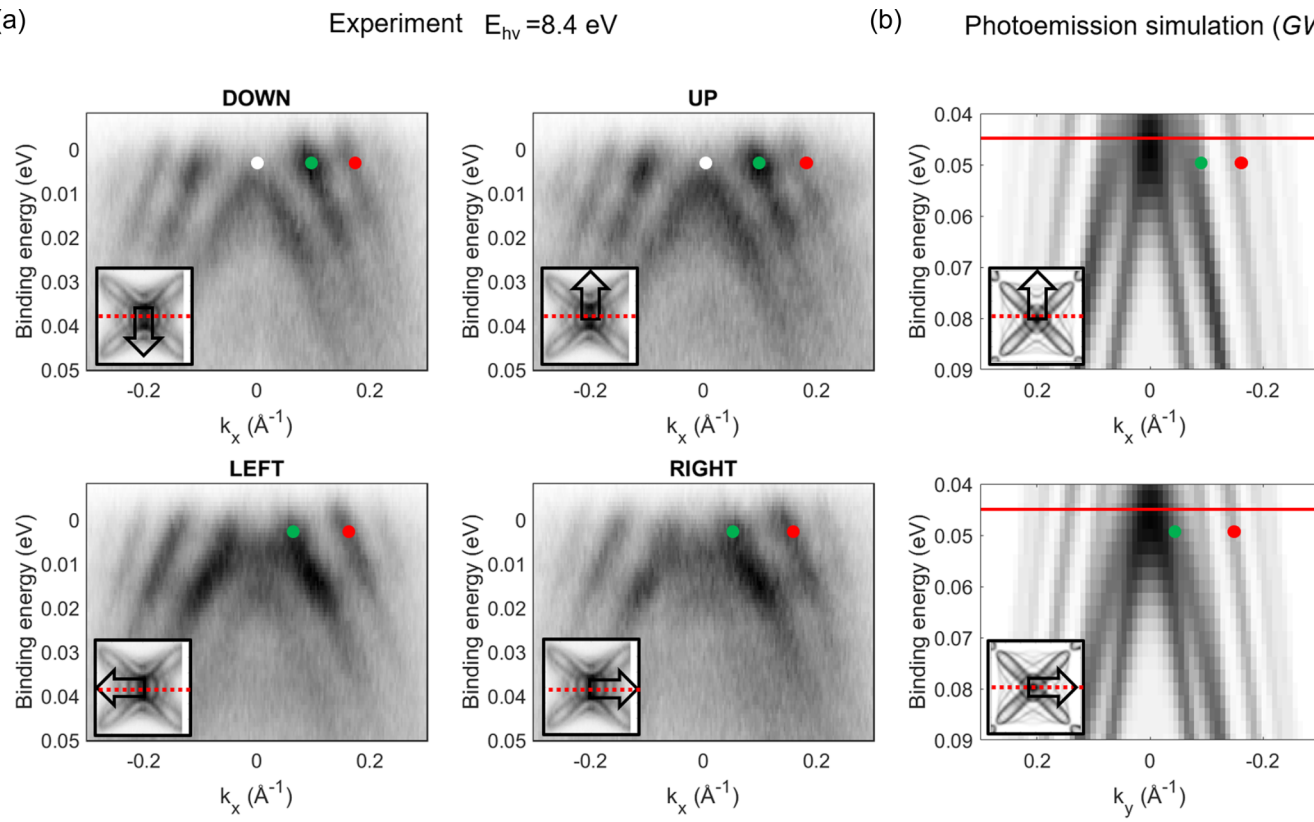

FIG. 8. (a) Experimental result obtained using unpolarized light of $E_{h\nu} = 8.4$ eV for a 40-ML-thick sample remanently magnetized along different in-plane directions. (b) Results of the corresponding photoemission simulations. Insets clarify the orientation of the cuts in k space (red dotted line) with respect to the magnetization direction (arrow). Red horizontal lines in (b) indicate position of the experimental Fermi level. Colored dots mark corresponding QWS.

between the dispersing states in the second case is visibly larger (compare the distance between the green and red dots). Upon the magnetization reversal, the QWS marked by a green dot moved $\Delta k \sim 0.03$ Å^{-1}, while the one marked by a red dot moved $\Delta k \sim 0.01$ Å^{-1}. The QWS marked by a white dot in the DOWN and UP spectra is barely visible for magnetizations LEFT and RIGHT. The associated shifts in the binding energy are of the order of 10 meV. These values are rather minute in comparison to the magnetization-dependent shifts observed before in thick Fe(001) films within the spin-orbit gap between bands 8 and 9 that were as large as $\Delta k = 0.1$ Å^{-1} and $\Delta E = 100$ meV [19]. The shifts within the QWS of bands 5 and 6 that we report here are reproduced by our simulation, also quantitatively [Fig. 8(b)]. This means that the observed effect is of the bulk origin and happens within the initial electronic band structure. In Ref. [13] it was suggested that strong anisotropy oscillations with a period of 8–10 ML in Fe/Au(001) multilayers might be related to electronic states that are split by spin-orbit interaction in the magnetization-dependent manner. Here we showed that these very states indeed change their position in energy and momentum when the magnetization direction is changed.

As the last point, we note that in the case of Fe we do not observe surface-derived states, which makes the comparison to the bulk calculation relatively straightforward. Still, there are some interesting features in the experimental result which are not explainable by our bulk-based simulation. For example, the experiment shows asymmetry between negative and positive k_x direction [Figs. 4(a) and 4(b), and Fig. 6(a) and 6(b)]. The most obvious source of this asymmetry is a spin-orbit gap between the bands 8 and 9. In Fig. 4(a) the gap is visible on the right-hand side of the image (within a black ellipsoid), while no gap is observed on the left-hand side. The gap changed location in k space when the magnetization direction was switched, keeping the same symmetry with respect to magnetization [Figs. 6(a) and 6(b), the gap is marked by a white ellipsoid]. The in-plane sample magnetization together with the broken translational symmetry due to the sample surface leads to the lowering of the rotational symmetry of the bulk states, leaving a single mirror plane perpendicular to the magnetization vector [19]. Consequently, this effect is not visible in the photoemission simulation, which does not include the surface-related effects [Fig. 6(d)]. We see that our photoemission simulation gives a very good starting point to analyze the deviations in the electronic dispersions close to the sample surface from the expectations for the pure bulk.

IV. SUMMARY AND CONCLUSIONS

We performed a thorough experimental study of the quantized electronic band structure of thin-film Fe(001)/Au(001) near the Fermi level. To identify the experimentally observed features, we performed photoemission simulations based on *GW* electronic band structure that take into account intrinsic

broadening along the $k_\perp$ direction and the spin degree of freedom. We obtained an extraordinary agreement between the experimental results and simulation within a wide photon energy range, also in terms of the spin polarization. We observed quantized states along the Δ direction, which could be responsible for the oscillations of the magnetic anisotropy with a period of ~ 5 and ~ 9 ML. We observed that these quantum well states change position in k space and energy depending on the magnetization direction. This effect is reproduced by our photoemission simulation which highlights its origin in the bulk initial electronic band structure of bcc Fe. Our photoemission simulation gives a good base to analyze the deviations of the surface electronic structure from the expectations for the pure bulk. We observed experimentally the magnetization-dependent spin-orbit gaps that reveal the symmetry breaking by the presence of the sample surface. We expect that the simulation method discussed in this work, which is simple yet powerful, might be helpful in understanding the photoemission intensities from other three-dimensional materials, especially when the spin-polarized quantized electronic states are considered.

ACKNOWLEDGMENTS

We thank C. Friedrich for valuable discussions. We gratefully acknowledge the computing time granted through JARA-HPC on the supercomputer JURECA at Forschungszentrum Jülich. This work was supported by the Helmholtz Association via The Initiative and Networking Fund, Alexander von Humboldt Foundation, and the statutory research funds of ICSC PAS within the subsidy of the Ministry of Science and Higher Education, Poland.

[1] T.-C. Chiang, Photoemission studies of quantum well states in thin films, Surf. Sci. Rep. **39**, 181 (2000).

[2] M. Milun, P. Pervan, and D. P. Woodruff, Quantum well structures in thin metal films: Simple model physics in reality? Reports Prog. Phys. **99**, 65 (2002).

[3] M. Bouhassoune, B. Zimmermann, P. Mavropoulos, D. Wortmann, P. H. Dederichs, S. Blügel, and S. Lounis, Quantum well states and amplified spin-dependent Friedel oscillations in thin films. Nat. Commun. **5**, 5558 (2014).

[4] P. Grünberg, R. Schreiber, Y. Pang, M. B. Brodsky, and H. Sowers, Layered Magnetic Structures: Evidence for Antiferromagnetic Coupling of Fe Layers across Cr Interlayers, Phys. Rev. Lett. **57**, 2442 (1986).

[5] M. N. Baibich, J. M. Broto, A. Fert, F. Nguyen Van Dau, F. Petroff, P. Etienne, G. Creuzet, A. Friederich, and J. Chazelas, Giant Magnetoresistance of (001)Fe/(001)Cr Magnetic Superlattices, Phys. Rev. Lett. **61**, 2472 (1988).

[6] S. Yuasa, T. Nagahama, and Y. Suzuki, Spin-polarized resonant tunneling in magnetic tunnel junctions, Science **297**, 234 (2002).

[7] T. Nagahama, S. Yuasa, Y. Suzuki, and E. Tamura, Quantum-well effect in magnetic tunnel junctions with ultrathin single-crystal Fe(100) electrodes, Appl. Phys. Lett. **79**, 4381 (2001).

[8] T. Nozaki, N. Tezuka, and K. Inomata, Quantum Oscillation of the Tunneling Conductance in Fully Epitaxial Double Barrier Magnetic Tunnel Junctions, Phys. Rev. Lett. **96**, 027208 (2006).

[9] M. Przybylski, M. Dabrowski, U. Bauer, M. Cinal, and J. Kirschner, Oscillatory magnetic anisotropy due to quantum well states in thin ferromagnetic films (invited), J. Appl. Phys. **111**, 07C102 (2012).

[10] J. Li, G. Chen, Y. Z. Wu, E. Rotenberg, and M. Przybylski, Quantum well states and oscillatory magnetic anisotropy in ultrathin Fe films, IEEE Trans. Magn. **47**, 1603 (2011).

[11] M. Dabrowski, T. R. F. Peixoto, M. Pazgan, A. Winkelmann, M. Cinal, T. Nakagawa, Y. Takagi, T. Yokoyama, F. Bisio, U. Bauer, F. Yildiz, M. Przybylski, and J. Kirschner, Oscillations of the Orbital Magnetic Moment Due to d-Band Quantum Well States, Phys. Rev. Lett. **113**, 067203 (2014).

[12] L. M. Sandratskii, Correlated oscillations of the magnetic anisotropy energy and orbital moment anisotropy in thin films: The role of quantum well states, Phys. Rev. B **92**, 134414 (2015).

[13] G. Y. Guo, Magnetocrystalline anisotropy oscillations predicted in Fe/Au(001) superlattices, J. Phys.: Condens. Matter **11**, 4329 (1999).

[14] J. Schäfer, M. Hoinkis, E. Rotenberg, P. Blaha, and R. Claessen, Spin-polarized standing waves at an electronically matched interface detected by Fermi-surface photoemission, Phys. Rev. B **75**, 092401 (2007).

[15] F. J. Himpsel, Fe on Au(100): Quantum-well states down to a monolayer, Phys. Rev. B **44**, 5966 (1991).

[16] Gerrit van der Laan, Microscopic origin of magnetocrystalline anisotropy in transition metal thin films, J. Phys.: Condens. Matter **10**, 3239 (1998).

[17] J.-P. Hanke, F. Freimuth, C. Niu, S. Blügel, and Y. Mokrousov, Mixed Weyl semimetals and low-dissipation magnetization control in insulators by spin-orbit torques, Nat. Commun. **8**, 1479 (2017).

[18] Peiheng Jiang, Lei Li, Zhaoliang Liao, Y. X. Zhao, and Zhicheng Zhong, Spin direction-controlled electronic band structure in two-dimensional ferromagnetic CrI3, Nano Lett. **18**, 3844 (2018).

[19] E. Młyńczak, M. Eschbach, S. Borek, J. Minár, J. Braun, I. Aguilera, G. Bihlmayer, S. Döring, M. Gehlmann, P. Gospodarič, S. Suga, L. Plucinski, S. Blügel, H. Ebert, and C. M. Schneider, Fermi Surface Manipulation by External Magnetic Field Demonstrated for a Prototypical Ferromagnet, Phys. Rev. X **6**, 041048 (2016).

[20] Daniel Gosálbez-Martínez, Ivo Souza, and David Vanderbilt, Chiral degeneracies and Fermi-surface Chern numbers in bcc Fe, Phys. Rev. B **92**, 085138 (2015).

[21] Daniel Gosálbez-Martínez, Gabriel Autès, and Oleg V. Yazyev, Topological Fermi-arc surface resonances in bcc iron, Phys. Rev. B **102**, 035419 (2020).

[22] A. Manchon, J. Železný, I. M. Miron, T. Jungwirth, J. Sinova, A. Thiaville, K. Garello, and P. Gambardella, Current-induced spin-orbit torques in ferromagnetic and antiferromagnetic systems, Rev. Mod. Phys. **91**, 035004 (2019).

[23] P. Moras, G. Bihlmayer, P. M. Sheverdyaeva, S. K. Mahatha, M. Papagno, J. Sánchez-Barriga, O. Rader, L. Novinec, S.

Gardonio, and C. Carbone, Magnetization-dependent Rashba splitting of quantum well states at the Co/W interface, Phys. Rev. B **91**, 195410 (2015).

[24] J. E. Ortega, F. J. Himpsel, G. J. Mankey, and R. F. Willis, Quantum-well states and magnetic coupling between ferromagnets through a noble-metal layer, Phys. Rev. B **47**, 1540 (1993).

[25] R. Matzdorf, UV-photoelectron spectroscopy at highest resolution—Direct access to lifetime effects in solids? Appl. Phys. A **63**, 549 (1996).

[26] V. N. Strocov, Intrinsic accuracy in 3-dimensional photoemission band mapping, J. Electron Spectrosc. Relat. Phenom. **130**, 65 (2003).

[27] W. Schattke, Photoemission within and beyond the one-step model, Prog. Surf. Sci. **54**, 211 (1997).

[28] Stefan Hüfner, *Photoelectron Spectroscopy* (Springer-Verlag, Berlin, 2003).

[29] Z. Tao, C. Chen, T. Szilvási, M. Keller, M. Mavrikakis, H. Kapteyn, and M. Murnane, Direct time-domain observation of attosecond final-state lifetimes in photoemission from solids, Science **353**, 62 (2016).

[30] Z. K. Liu, B. Zhou, Y. Zhang, Z. J. Wang, H. M. Weng, D. Prabhakaran, S.-K. Mo, Z. X. Shen, Z. Fang, X. Dai, Z. Hussain, and Y. L. Chen, Discovery of a three-dimensional topological Dirac semimetal, Na_3Bi, Science **343**, 864 (2014).

[31] H. J. Elmers, D. Kutnyakhov, S. V. Chernov, K. Medjanik, O. Fedchenko, A. Zaporozhchenko-Zymakova, M. Ellguth, C. Tusche, J. Viefhaus, and G. Schönhense, Hosting of surface states in spin–orbit induced projected bulk band gaps of W(110) and Ir(111), J. Phys.: Condens. Matter **29**, 255001 (2017).

[32] E. Młyńczak, M. C. T. D. Müller, P. Gospodarič, T. Heider, I. Aguilera, G. Bihlmayer, M. Gehlmann, M. Jugovac, G. Zamborlini, C. Tusche, S. Suga, V. Feyer, L. Plucinski, C. Friedrich, S. Blügel, and C. M. Schneider, Kink far below the Fermi level reveals new electron-magnon scattering channel in Fe, Nat. Commun. **10**, 505 (2019).

[33] C. Tusche, M. Ellguth, V. Feyer, A. Krasyuk, C. Wiemann, J. Henk, C. M. Schneider, and J. Kirschner, Nonlocal electron correlations in an itinerant ferromagnet, Nat. Commun. **9**, 3727 (2018).

[34] P. M. Sheverdyaeva, R. Requist, P. Moras, S. K. Mahatha, M. Papagno, L. Ferrari, E. Tosatti, and C. Carbone, Energy-momentum mapping of d-derived Au(111) states in a thin film, Phys. Rev. B **93**, 035113 (2016).

[35] C. Carbone, P. Moras, P. M. Sheverdyaeva, D. Pacilé, M. Papagno, L. Ferrari, D. Topwal, E. Vescovo, G. Bihlmayer, F. Freimuth, Y. Mokrousov, and S. Blügel, Asymmetric band gaps in a Rashba film system, Phys. Rev. B **93**, 125409 (2016).

[36] J. H. Dil, F. Meier, J. Lobo-Checa, L. Patthey, G. Bihlmayer, and J. Osterwalder, Rashba-Type Spin-Orbit Splitting of Quantum Well States in Ultrathin Pb Films, Phys. Rev. Lett. **101**, 266802 (2008).

[37] P. Gospodarič, E. Młyńczak, M. Eschbach, M. Gehlmann, G. Zamborlini, V. Feyer, L. Plucinski, and C. M. Schneider, Localized segregation of gold in ultrathin Fe films on Au(001), Phys. Rev. B **97**, 085409 (2018).

[38] C. Tusche, A. Krasyuk, and J. Kirschner, Spin resolved bandstructure imaging with a high resolution momentum microscope, Ultramicroscopy **159**, 520 (2015).

[39] C. Tusche, M. Ellguth, A. A. Ünal, C.-T. Chiang, A. Winkelmann, A. Krasyuk, M. Hahn, G. Schönhense, and J. Kirschner, Spin resolved photoelectron microscopy using a two-dimensional spin-polarizing electron mirror, Appl. Phys. Lett. **99**, 032505 (2011).

[40] C. Tusche, M. Ellguth, A. Krasyuk, A. Winkelmann, D. Kutnyakhov, P. Lushchyk, K. Medjanik, G. Schönhense, and J. Kirschner, Quantitative spin polarization analysis in photoelectron emission microscopy with an imaging spin filter, Ultramicroscopy **130**, 70 (2013).

[41] A. Kokalj, Computer graphics and graphical user interfaces as tools in simulations of matter at the atomic scale, Comput. Mater. Sci. **28**, 155 (2003).

[42] A. Mugarza, J. E. Ortega, A. Mascaraque, E. G. Michel, K. N. Altmann, and F. J. Himpsel, Periodicity and thickness effects in the cross section of quantum well states, Phys. Rev. B **62**, 12672 (2000).

[43] M. A. Mueller, T. Miller, and T.-C. Chiang, Determination of the bulk band structure of Ag in Ag/Cu(111) quantum-well systems, Phys. Rev. B **41**, 5214 (1990).

[44] http://www.flapw.de.

[45] C. Friedrich, S. Blügel, and A. Schindlmayr, Efficient implementation of the GW approximation within the all-electron FLAPW method, Phys. Rev. B **81**, 125102 (2010).

[46] N. Marzari, A. A. Mostofi, J. R. Yates, I. Souza, and D. Vanderbilt, Maximally localized Wannier functions: Theory and applications, Rev. Mod. Phys. **84**, 1419 (2012).

[47] A. A. Mostofi, J. R. Yates, Y.-S. Lee, I. Souza, D. Vanderbilt, and N. Marzari, wannier90: A tool for obtaining maximally-localised Wannier functions, Comput. Phys. Commun. **178**, 685 (2008).

[48] C. Friedrich, A. Schindlmayr, S. Blügel, and T. Kotani, Elimination of the linearization error in GW calculations based on the linearized augmented-plane-wave method, Phys. Rev. B **74**, 045104 (2006).

[49] J. D. Riley, A. L. Walter, and O. Rader, Theoretical limitations to the determination of bandwidth and electron mass renormalization: The case of ferromagnetic iron, New J. Phys. **12**, 013007 (2010).

[50] M. P. Seah and W. A. Dench, Quantitative electron spectroscopy of surfaces: A standard data base for electron inelastic mean free paths in solids, Surf. Interface Anal. **1**, 2 (1979).

[51] S. Moser, An experimentalist's guide to the matrix element in angle resolved photoemission, J. Electron Spectros. Relat. Phenom. **214**, 29 (2017).

[52] F. J. Himpsel, J. E. Ortega, G. J. Mankey, and R. F. Willis, Magnetic nanostructures, Adv. Phys. **47**, 511 (1998).